



HAL
open science

Mutagenesis of Dimer Interfacial Residues Improves the Activity and Specificity of Methyltransferase for cis- α -Irone Biosynthesis

Rehka T., Xin Li, Jing Sen Ong, Jérémy Esque, Congqiang Zhang, Qingsong Lin, Isabelle André, Xixian Chen

► To cite this version:

Rehka T., Xin Li, Jing Sen Ong, Jérémy Esque, Congqiang Zhang, et al.. Mutagenesis of Dimer Interfacial Residues Improves the Activity and Specificity of Methyltransferase for cis- α -Irone Biosynthesis. Journal of Agricultural and Food Chemistry, 2023, 71 (22), pp.8497-8507. 10.1021/acs.jafc.3c01272 . hal-04251978

HAL Id: hal-04251978

<https://hal.insa-toulouse.fr/hal-04251978>

Submitted on 20 Oct 2023

HAL is a multi-disciplinary open access archive for the deposit and dissemination of scientific research documents, whether they are published or not. The documents may come from teaching and research institutions in France or abroad, or from public or private research centers.

L'archive ouverte pluridisciplinaire **HAL**, est destinée au dépôt et à la diffusion de documents scientifiques de niveau recherche, publiés ou non, émanant des établissements d'enseignement et de recherche français ou étrangers, des laboratoires publics ou privés.

Mutagenesis of Dimer Interfacial Residues Improves the Activity and Specificity of Methyltransferase for *cis*- α -Irone Biosynthesis

Rehka T., Xin Li, Jing Sen Ong, Jérémy Esque, Congqiang Zhang, Qingsong Lin, Isabelle André, and Xixian Chen*

ABSTRACT: Promiscuous enzymes show great potential to establish new-to-nature pathways and expand chemical diversity. Enzyme engineering strategies are often employed to tailor such enzymes to improve their activity or specificity. It is paramount to identify the target residues to be mutated. Here, by exploring the inactivation mechanism with the aid of mass spectrometry, we have identified and mutated critical residues at the dimer interface region of the promiscuous methyltransferase (pMT) that converts psi-ionone to irone. The optimized pMT12 mutant showed ~ 1.6 – 4.8 -fold higher k_{cat} than the previously reported best mutant, pMT10, and increased the *cis*- α -irone percentage from ~ 70 to $\sim 83\%$. By one-step biotransformation, ~ 121.8 mg L⁻¹ *cis*- α -irone was produced from psi-ionone by the pMT12 mutant. The study offers new opportunities to engineer enzymes with enhanced activity and specificity.

KEYWORDS: methyltransferase, irone, enzyme engineering, suicide inactivation, proteomic analysis

■ INTRODUCTION

S-Adenosylmethionine (SAM)-dependent methyltransferases play an important role in diversifying natural products and changing their biological activities.^{1,2} Majority of methyltransferases undergo the S_N2-type nucleophilic substitution reaction in which the methyl group is donated to a variety of electron-rich chemical groups. This reaction mechanism has been harnessed to introduce structural diversity to natural products and expand the biosynthetic capacity. Many methyltransferases have been engineered to accept non-native substrates,^{3–5} produce alternative products,^{2,6} and introduce a different donor group.^{7,8} Recently, we have tailored a promiscuous methyltransferase (pMT) to convert psi-ionone to irone, a premium flavor and fragrance molecule.³ By mutating the active site residues, we generated the pMT7 mutant, containing Y200F, S182E, L273V, L180A, A202L, and Y65F mutations, which was the most specific toward *cis*- α -irone production from psi-ionone. With additional C156A and T91P mutations, we obtained the pMT10 mutant, which was more active but less specific than pMT7. The next step to consider is thus either to improve the activity of pMT7 or the specificity of pMT10 to further increase *cis*- α -irone production.

To achieve that, we seek to understand the inactivation mechanism of the methyltransferase, which has led to an improved P450-catalyzed cyclopropanation reaction.⁹ Indeed, there have been reports showing that certain methyltransferases undergo suicide inactivation during catalysis. For example, thioether S-methyltransferase is inactivated by its product, methyl ethyl vinyl sulfonium ion, which becomes electrophilic and forms a covalent bond with the enzyme.¹⁰

The O⁶-methylguanine-DNA methyltransferase is also rapidly inactivated through methylation of a cysteine residue, since the O⁶-methyl moiety of methylguanine is susceptible to nucleophilic attack.¹¹ Drug candidates are designed to inhibit methyltransferases by employing a similar inactivation mechanism whereby electrophilic products or intermediates form covalent interactions with the enzymes.¹² In our case, an electrophilic intermediate is generated during the methyl group transfer from SAM to psi-ionone, which could lead to covalent modification of the pMT enzyme.

In this study, we performed an intact protein and proteomic study on the pMT7 mutant using mass spectrometry to identify if such an inactivation pathway exists so as to pinpoint the residues to be mutated for improved activity. Interestingly, we discovered that an amino acid residue, Q60, near the dimer interface region and far away from the active site was involved in facilitating a strong interaction between psi-ionone and the pMT enzyme. Mutating Q60 to valine based on the pMT7 mutant was found to increase k_{cat} by ~ 2 -fold. Structural analysis suggested that Q60V mutation alters the interaction network between the residue and the dimer interchain loop (W41-M52) and plays a role in the stabilization of the enzyme. This led us to identify an additional amino acid residue N231

also involved in the stabilization of the loop via hydrogen bonding interactions. The N231D mutation increased pMT10 specificity and improved the percentage of *cis*- α -irone in the product mixture from ~70 to ~83%. By combining different mutations, the final best mutant, pMT12, increased *cis*- α -irone production by ~4.7- and 1.3-fold compared to pMT7 and pMT10, respectively, resulting in a final concentration of ~121.8 mg L⁻¹ from psi-ionone. These findings bring us one step closer to the development of a biotechnological process to produce irone from a simple carbon source.

MATERIALS AND METHODS

Strains, Plasmids, and Chemicals. The strains and plasmids utilized were similar to our previous study.³ *Escherichia coli* BL21-Gold DE3 strain (Stratagene) was used in this study. The CRASH protocol was used to modify the *E. coli* genome.¹³ The pMT gene was subcloned into a pET-11a vector (Invitrogen). For in vivo production, the enzymes were cloned into plasmids with the modified p15A origin of replication (Supporting Table S1).¹⁴ *MtaD* from *Thermotoga maritima* was codon-optimized and synthesized by Integrated DNA Technologies, Inc., while *Mtn* and *MetK* were amplified from the *E. coli* genome. Unless otherwise specified, all chemicals were procured from Sigma-Aldrich.

Site-Directed Mutagenesis with a Robotics Platform. Restriction-free (RF) cloning methods were employed to construct the site-directed mutations¹⁴ and the protocol has been adapted to be performed on an integrated automation platform (Molecular Devices). In brief, overlapping primers that carried the desired mutation were designed to amplify the pMT gene. A 10 μ L PCR reaction was assembled according to an iProof High-Fidelity DNA Polymerase Kit (Bio-Rad # 1725330) on TwinTec skirted PCR Plates (Eppendorf #30128648) using the Beckman Coulter Biomek i7 liquid handler. The PCR plate was moved to an on-deck thermal cycler (INHECO) by the PreciseFlex PF400 robot arm to carry out the PCR reaction. Subsequently, the plate was returned to the Biomek liquid handler, and 1 μ L of the *DpnI* enzyme (NEB # R0176) was added and incubated at 37 °C for 3 h to digest the template DNA. Following that, 1 μ L of the *DpnI*-treated PCR product was mixed with 10 μ L of DH5 α chemical competent cells (ECOS 101, Yeastern Biotech #FYE609-80VL) in a full-skirt round-bottom 96-well standard plate (Greiner #650180) and kept on a cooled Peltier surface at 4 °C for 5 min in the Biomek liquid handler. Heat shock was performed by quickly moving the plate by the gripper to the heating station at 42 °C for 45 s and moving back to the 4 °C Peltier surface for another 2 min. 100 μ L of the LB medium was added and the plate was moved to a shaking incubator (Liconic STX44-1CBT) with the shaking speed set at 30% power (~300 rpm) at 37 °C to rescue the cells for 1 h. Subsequently, 25 μ L of the rescued cells were plated onto LB agar supplemented with 100 mg L⁻¹ ampicillin in an 8-well agar tray (Thermo Fisher Nunc OmniTray8 #267062) using the Molecular Devices QPix HT Colony Picker System (QPix 420). OmniTrays were moved manually to a 37 °C incubator to allow for colonies to form. After overnight incubation, a single colony was picked by QPix and inoculated into 1 mL of LB medium in a 96-well U-bottom deep-well plate (Bio Basic # CDP0011-F) and cultured at 37 °C overnight at 1200 rpm on a benchtop microplate incubator (Atlantis Bioscience # ES-60E). The plasmids were then extracted using a Mag-Bind Ultra-Pure Plasmid DNA 96 Kit (Omega BioTek #M1258-01) on the Biomek liquid handler following the manufacturer's protocol with a magnetic plate adaptor (Beckman Coulter #A32782). All of the plasmids were sequence-confirmed before using them for protein expression and activity tests.

Purified Enzyme Reactions for Characterization and Proteomics Study. His-tag protein purification was performed using the same method previously described³ and according to the manufacturer's instructions (Cube Biotech # 31105). Subsequently, a 100 μ L enzymatic reaction (100 mM Tris (pH 7), 10 mM MgCl₂, 100 mM NaCl, 0.5 mg mL⁻¹ purified enzyme, 40 mg L⁻¹ psi-ionone, 0.2

mM SAM (Aaron chemicals #I003035)) was set up and incubated at 28 °C overnight. 100 μ L of ethyl acetate (VWR #VWRC83621.320) was used to extract *cis*- α -irone and leftover psi-ionone and analyzed by gas chromatography–mass spectrometry (GCMS). For kinetics, the same enzymatic reaction condition was used. Psi-ionone concentration was varied from 2 to 40 mg L⁻¹ while keeping SAM at 0.2 mM; SAM concentration was varied from 2 to 200 μ M while keeping psi-ionone at 40 mg L⁻¹. The reactions were stopped after 1 h at 28 °C, 1200 rpm, and extracted with ethyl acetate.

For intact protein analysis, two sets of 1 mL enzymatic reactions were set up in 20 mL headspace solid-phase microextraction (HS–SPME) vials (Thermo Fisher #18091307). All reactions consisted of a final concentration of 10 mM Tris (pH 7), 10 mM MgCl₂, 15 mM NaCl, and 8 mg mL⁻¹ purified pMT7. The reactions were incubated overnight at 28 °C, 300 rpm. For samples with substrates, it was set up with 40 mg L⁻¹ psi-ionone and 0.2 mM SAM. For other samples without substrates, neither psi-ionone nor SAM was added. The overnight reactions were then extracted with 1 mL of ethyl acetate, vortexed, and transferred into a 2 mL tube. The samples were vortexed for 10–15 min at room temperature before spinning down at 21130g for 10 min. From the organic layer, 200 μ L was taken for GCMS analysis. The 1 mL aqueous layer was passed through a PD 10 desalting column (Cytiva #17085101) and eluted with 20 mM ammonium acetate (pH 7). Following that, the eluted fraction was concentrated to ~1 mg mL⁻¹ using a 10 kDa MWCO ultracentrifugal spin column (Vivaspin #28932360), reconstituted with 10% acetonitrile with 0.1% formic acid, and subjected to intact protein analysis. For proteomics analysis, 10 reactions with substrates, 1 mL each, were set up and the aqueous layers were pooled together for desalting and subjected to protein fractionation.

Preparation of Cell Lysates and Enzymatic Reactions with Cell Lysates. Similar to our previous study,³ BL21 cells transformed with the pMT mutant were directly grown in 10 mL of autoinduction media at 20 °C, 300 rpm. Then, the cells were collected and resuspended in 1 mL of PBS. Equal cell amounts (namely, 24,000 μ L of OD cells) were collected and resuspended in 600 μ L of lysis buffer (10 mM Tris (pH 7), 2.5 mM MgCl₂, 0.5 mM CaCl₂, 150 mM NaCl, 1 mg mL⁻¹ lysozyme, 0.5% glycerol, and 20 U mL⁻¹ DNaseI (NEB #M0303L)). Cell lysis was carried out first with lysozyme treatment at 20 °C, 300 rpm for 1 h, followed by two cycles of freeze–thaw: cells were frozen at –80 °C overnight and then thawed at room temperature for ~1 h. After the second thawing, 500 μ L of cell lysate was added to a 1 mL reaction (50 mM Tris (pH 7), 10 mM MgCl₂, 60 mM NaCl, 0.2 mM SAM and 40 mg L⁻¹ of psi-ionone) in 1.5 mL GC vials (Thermo Fisher #11090500). The reaction was carried out at 28 °C and 300 rpm for 2–3 days and extracted with 500 μ L of ethyl acetate.

Biotransformation of Glucose/Glycerol into *cis*- α -Irone. Plasmids carrying the pathway enzymes were transformed into 2O31 and 2O31 Δ *metJ* strains (Supporting Table S1) and spread on LB agar plates supplemented with 100 mg L⁻¹ spectinomycin, 34 mg L⁻¹ chloramphenicol, 100 mg L⁻¹ ampicillin, and 50 mg L⁻¹ kanamycin. Three random colonies were inoculated into 1 mL of LB media with antibiotics. Cells at 0.1 OD from the overnight culture were then inoculated into 1 mL of chemically defined autoinduction media in a 20 mL HS–SPME vial.³ The culture was cultivated at 28 °C for 72 h and was extracted with 1 mL of ethyl acetate for GCMS analysis.

Gas Chromatography–Mass Spectrometry Analysis. The extracted products were analyzed with an Agilent Intuvo 9000 gas chromatograph coupled with an Agilent 5977B mass spectrometer and an Agilent DB-WAX Ultra Inert Intuvo GC column (30 m \times 250 μ m \times 0.25 μ m). The oven program was as follows: initially held at 50 °C for 1 min, then increased to 200 °C at a rate of 40 °C min⁻¹ and held at 200 °C for 3 min, and finally increased to 230 °C at a rate of 40 °C min⁻¹ and held at 230 °C for 5 min. The compound concentration was calculated against an external standard curve.

Intact Protein Analysis and Proteomics Study. The analysis of the pMT7 samples was performed on a Waters Synapt G2-Si system, and data were processed using MaxEnt 1 software.¹⁵ The

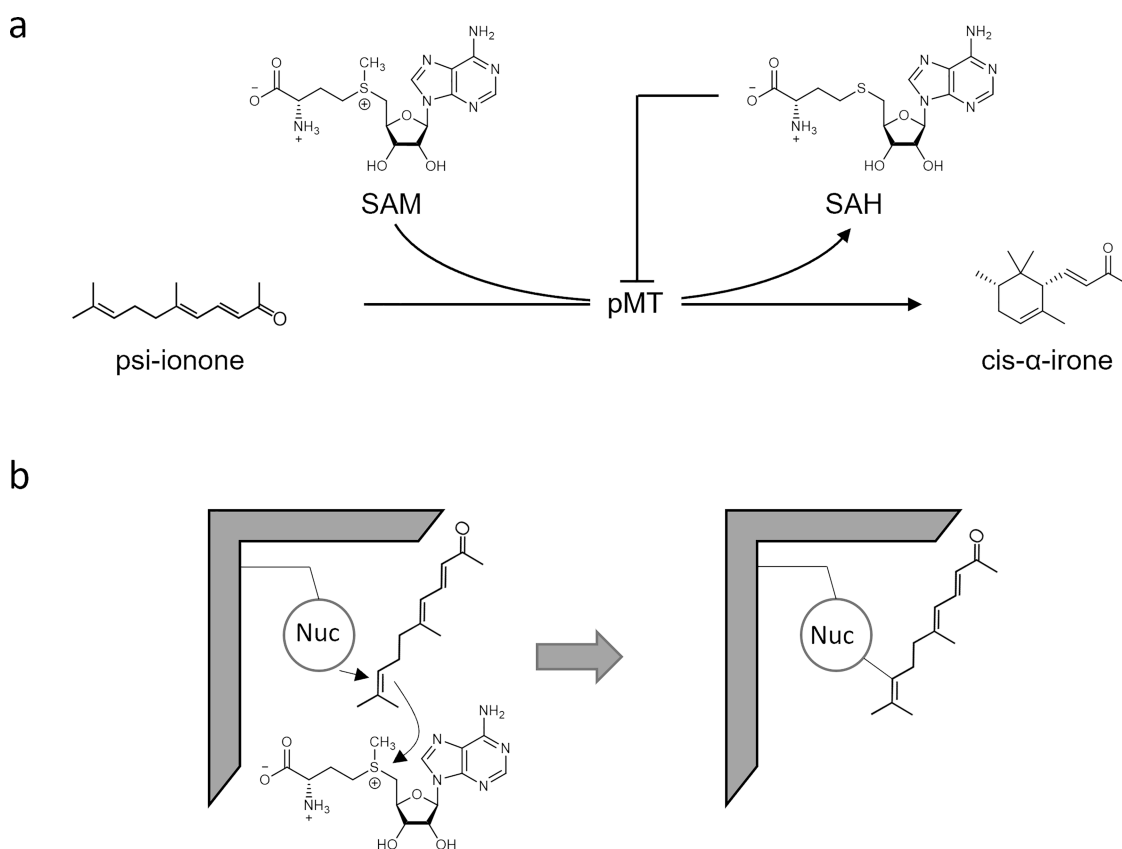


Figure 1. Schematic illustration of the promiscuous methyltransferase reaction and the hypothesized inactivation mechanism. (a) The pMT reaction that converts psi-ionone and SAM into *cis- α -irone* and SAH. The enzyme activity is inhibited by the byproduct, SAH. (b) An inactivation reaction mechanism was proposed that pMT might be covalently modified during the nucleophilic substitution reaction to form an inactive complex. The enzyme is represented as a gray shape and the nucleophile is represented as a blue circle.

experimental parameters were as follows: desolvation gas temperature: 400 °C; source temperature: 80 °C; capillary voltage: 3 kV; cone gas flow: 40 L h⁻¹; desolvation gas flow: 800 L h⁻¹; source offset: 40; sampling cone: 40.

The modified pMT7 were offline fractionated using an Agilent 1260 UHPLC. The collected fraction containing the modified pMT7 was then tryptic digested and analyzed on a SCIEX TripleTOF 5600 system coupled with an Eksigent NanoLC-Ultra with a Thermo Scientific Acclaim PepMap100 C18 column (3 μ m 100 Å, 75 μ m \times 250 mm). The settings were as follows: IonSpray voltage: 2.3 kV; interface heater temperature: 150 °C; curtain gas: 30 units; nebulizer gas: 10 units; MS1 mass range: 350–1250 *m/z*, MS2 mass range: 100–1800 *m/z*. The data was searched using ProteinPilot 5.0.

The analysis of Q60V was done on a Q Exactive Plus Orbitrap Biopharma system coupled with Vanquish UHPLC. Spectra recorded were analyzed by Thermo BioPharma Finder software. The samples were analyzed on a 10 cm Thermo Scientific MAbPac column using a 12 min gradient. The following experimental parameters were used on the Orbitrap platform: the instrument was calibrated externally using Thermo Scientific Pierce Calibration Solutions. The source was operated in the positive mode, the capillary voltage was set to 3.8 kV, the capillary temperature was 320 °C, and the protein mode was on with pressure at 0.2. MS spectra were recorded at a resolution of 17,500.

Computational Studies. The three-dimensional structures from our previous study³ were used to generate models for pMT7, pMT7_Q60V, pMT12, and pMT12_Q60V. One dimeric unit was used, which was complex with 1RS for *cis- α -irone* and SAH. All mutants were modeled using Modeller and three-dimensional (3D) models with the lowest DOPE score were kept for further analyses.¹⁶ Molecular dynamics (MD) simulations were performed using the AMBER ff14S force field¹⁷ for enzymes and GAFF¹⁸ for the ligands

using pmemd.CUDA of AMBER18 software.¹⁹ The partial charges for the ligand were computed using the AM1-BCC method²⁰ from an antechamber. The system was protonated using propka web server to set the experimental pH of 7. MD simulation parameters were as follows:³ in all stages, the sulfur of SAH was kept close to the key carbon irone C4 isomer using the NMR distance restraint algorithm, with the following parameters on the distance in Å (r1 = 0, r2 = 0, r3 = 4, r4 = 5) and following parameters on the force constant in kcal mol⁻¹ Å⁻² (rk2 = 0, rk3 = 25.0). The MD simulations were carried out for a total of 100 ns for all complexes, with the two active sites occupied by the ligands (SAH and *cis- α -irone* 1RS). MM/PBSA calculations were performed using MMPBSA.py software and default parameters for Poisson–Boltzmann as described by Miller et al.²¹ Weblogo was built in three steps: (i) 76 first residues of the wild-type methyltransferase (PDB ID: 5GM2) were blasted using the blastp server and only sequences having more than 90% of coverage were picked up. (ii) Multiple sequence alignment (MSA) was performed using MAFFT.²² (iii) Weblogo server (<https://weblogo.berkeley.edu/logo.cgi>) was used to build the web logo only on the sequence of interest, which is SSQAQDRY.²³

RESULTS AND DISCUSSION

Mass Spectrometry-Assisted Identification of the Target Residue. Previously, we have identified a promiscuous methyltransferase (pMT) that converts psi-ionone to *cis- α -irone*.³ Following a structure-guided enzyme engineering strategy, we obtained the pMT7 mutant, containing Y200F, S182E, L273V, L180A, A202L, and Y65F mutations, which produced the highest percentage of *cis- α -irone*. While characterizing pMT7, we noticed that the enzymatic activity reached a plateau before the significant conversion was

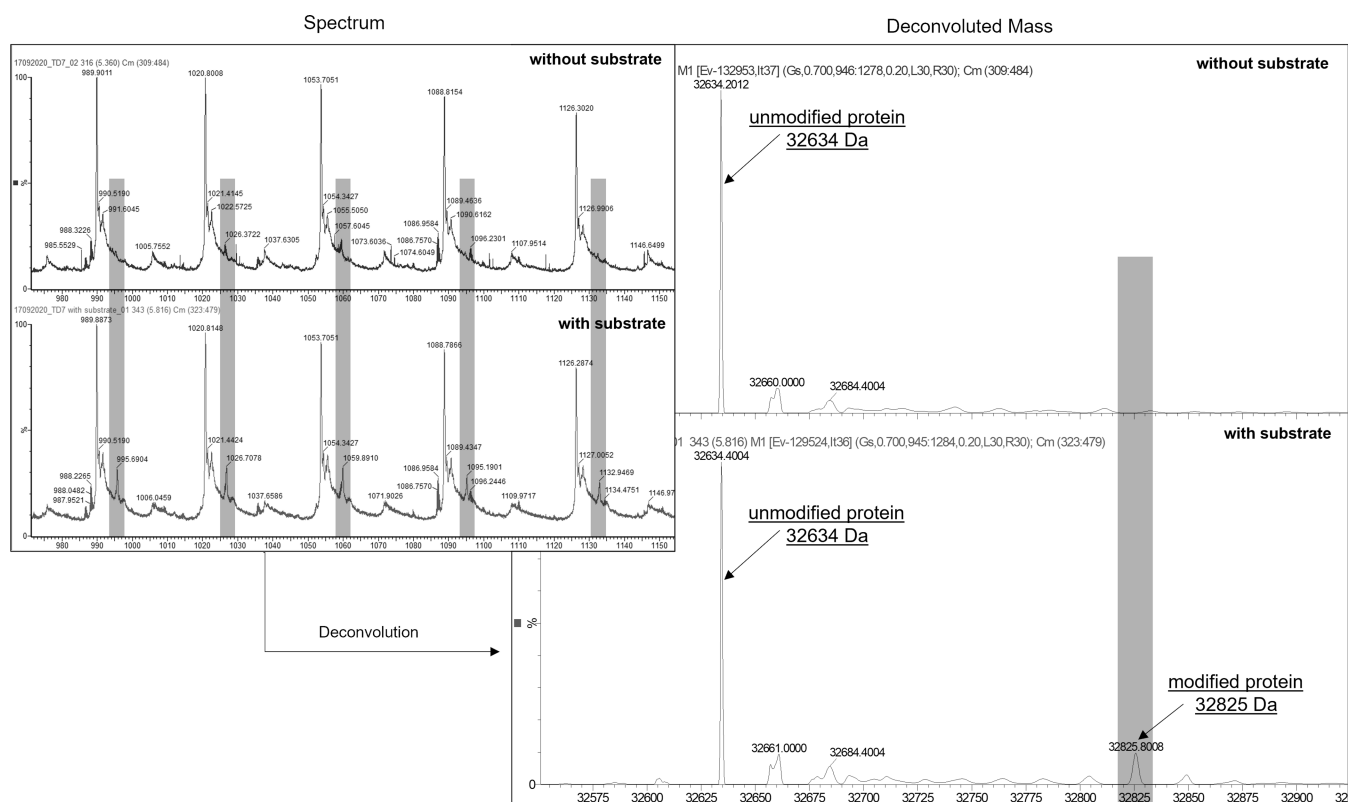


Figure 2. Mass spectrum and deconvoluted mass of pMT7 incubated without or with substrates by intact protein mass analysis. The major mass obtained is 32634 Da, which corresponds to the unmodified protein. An additional proteoform with a mass of 32825 Da was highlighted in gray, which is only detected in samples with the substrate.

achieved. It was partially attributed to the feedback inhibition from the byproduct, *S*-adenosylhomocysteine (SAH, [Figure 1a](#)). However, the amount of SAH ($\sim 0.2 \mu\text{M}$) produced was 10 times lower than the IC_{50} value of SAH to pMT7. Hence, other inactivation pathways could exist that are yet to be explored. It is known that some methyltransferases undergo suicide inactivation with an electrophilic intermediate or a product, and some drugs or non-native substrates are designed based on such a mechanism.^{10,12} We then hypothesized that pMT7 was also modified during the nucleophilic reaction, since its active site was reshaped through mutations and psionone, a non-native substrate, was used ([Figure 1b](#)). Intact protein mass analysis under denaturing conditions was performed with the purified pMT7 enzyme incubated with or without the substrates (psi-ionone and SAM). As shown in [Figure 2](#), the average mass of the major proteoform was determined to be 32,634 Da, which is the mass of the unmodified protein. An additional proteoform with a mass of 32,825 Da was also detected only in the sample with the substrate, suggesting that a fraction of the protein might have been modified during the reaction. Moreover, the mass difference between the modified and unmodified proteins is 191.4 Da, which is ~ 1 proton mass less than the mass of psionone (192.3 Da). This suggested a strong interaction, or the possible formation of a covalent bond between the non-native substrate and pMT7, which might have substituted one of the C–H bonds in psionone or pMT7 ([Figure 1b](#)). To identify the residues that are involved in the interaction, the protein from the overnight reaction was separated into unmodified and modified protein fractions, digested with trypsin, and subjected to proteomic analysis. A peptide fragment SSQAQDRFTDY-

LIETLDPK (residues 58–76) with possible modification at the glutamine was detected ([Figure 3a](#)). However, the exact modification site remains unclear, since there are two glutamines in the sequence.

Mutagenesis of Dimer Interchain Residues Improved Enzyme Activity. Based on the crystallographic structure, the peptide is located near the dimer interface ([Figure 3b](#)). The side chain of Q60 points away from the active site and forms hydrogen bonding interactions with the backbone of the loop at the dimer interface (residues W41-M52). On the other hand, Q62 is orientated toward the active site, suggesting that it could have a more drastic effect on enzymatic activity and could be the site of modification. Moreover, by blasting this sequence, we noticed that Q60 is variable and the most predominant amino acid residues are R, Q, and L ([Figure 3c](#)). In agreement with structural analysis, Q62 is more conserved with few sequences replacing glutamine (Q) with methionine (M), highlighting the importance of this residue.

Site saturation mutagenesis was then carried out on both glutamines, Q60 and Q62 in the pMT7 template using our in-house robotics platform. For the initial screen, the plasmids carrying different pMT7 variants were transformed into psionone accumulating *E. coli* 2O31, and the *cis*- α -irone concentration was quantified by GCMS ([Supporting Figure S1](#)). From the analysis, Q62 appears clearly critical to the enzymatic activity, as most of the mutations on Q62 resulted in a drastic decrease in irone production. In comparison, there were three beneficial mutations based on Q60: Q60V, Q60K, and Q60R that improved *cis*- α -irone production by ~ 1.6 -, ~ 1.3 -, and 1.4-fold, respectively, compared to pMT7. This somewhat agrees with the sequence alignment analysis. To rule

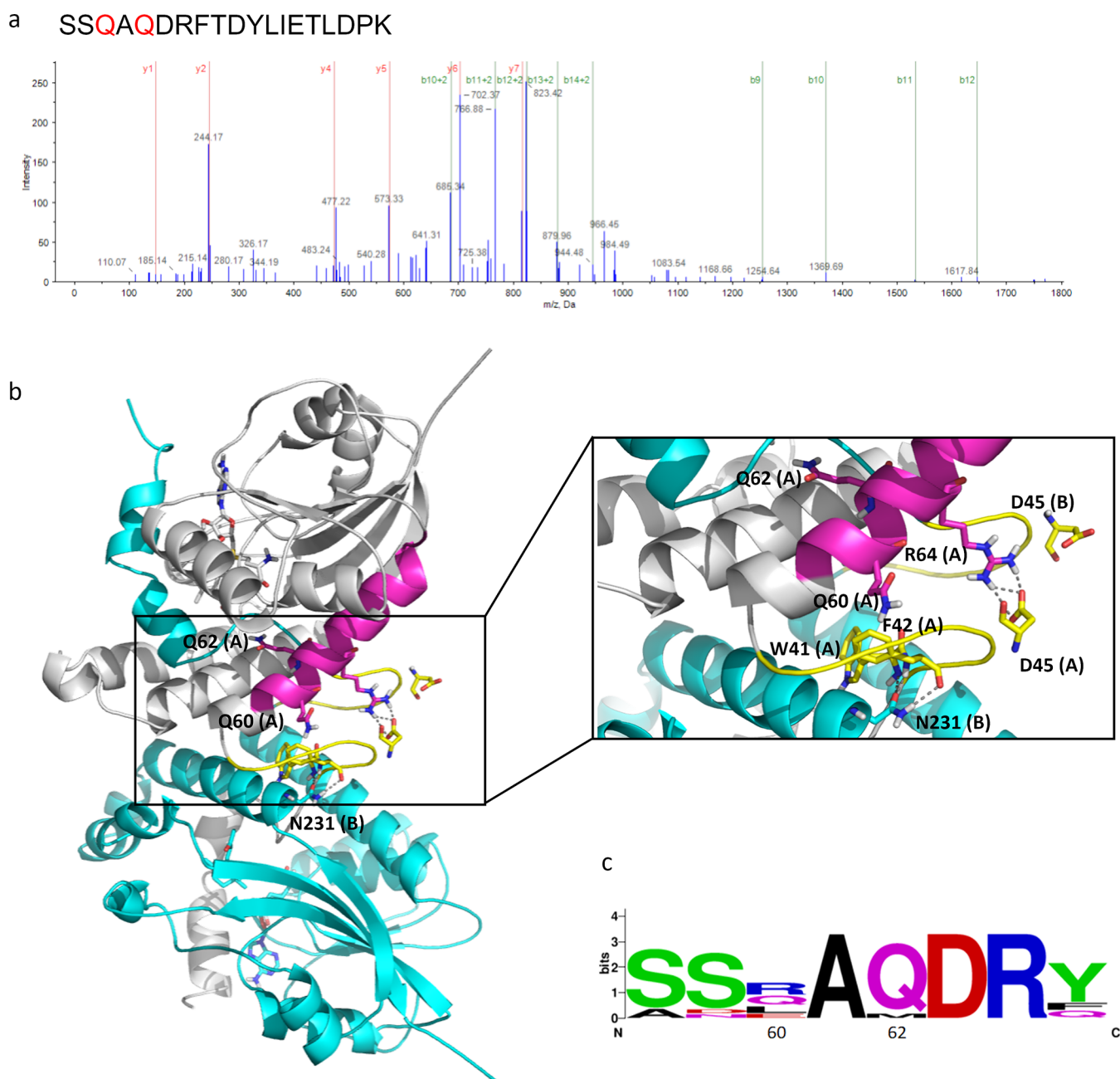


Figure 3. Identification of the residues involved in the strong interaction between pMT7 and psi-ionone. (a) Proteomics analysis of the modified and unmodified pMT7 enzyme fractions after being treated with trypsin. The possible modified glutamine residues are indicated in red. (b) One dimeric unit of the pMT7 enzyme is shown as a cartoon representation. One monomer is in white (chain A) and the other in cyan (chain B). IRS for *cis*- α -irone and SAH are shown as sticks in the active site of their respective chains. The modified glutamine residues are highlighted as sticks. The hydrogen bonds are shown as gray dotted lines. The dimer interchain loop region is shown as an enlarged view with the W41-M52 loop shown in yellow and the peptide fragment SSQAQDRFTDYLIETLDPK (residues 58–76) from chain A in magenta. The amino acid residues that are involved in the interaction networks are labeled with a single letter with the chain number indicated in the bracket. (c) Web logo representation of the peptide fragment region (residues 58–79).²³

out that the improved irone production was not a result of unequal psi-ionone supply, we then assayed the three positive mutants using cell lysates with the same amounts of synthetic psi-ionone. As shown in Figure 4a, Q60V mutation increased the methyltransferase activity by ~50%, whereas Q60K or Q60R mutation reduced the methyltransferase activity. This indicates that Q60 mutations might have affected the pathway balance and hence psi-ionone production during *in vivo* assay. Next, to further confirm that the improved activity is not a result of the improved expression, we purified pMT7_Q60V

and characterized the enzyme *in vitro*. The k_{cat} of pMT7_Q60V increased by ~2-2.5-fold compared to pMT7 (Table 1). Moreover, the K_m value of pMT7_Q60V for psi-ionone increased by >2-fold compared to that of pMT7, suggesting a lower binding interaction between psi-ionone and the enzyme after introduction of Q60V mutation (Table 1). Interestingly, we found no difference in the proteoform of purified pMT7_Q60V incubated with or without the substrates by intact protein analysis (Figure 4b), indicating that the possible modification by psi-ionone observed in pMT7

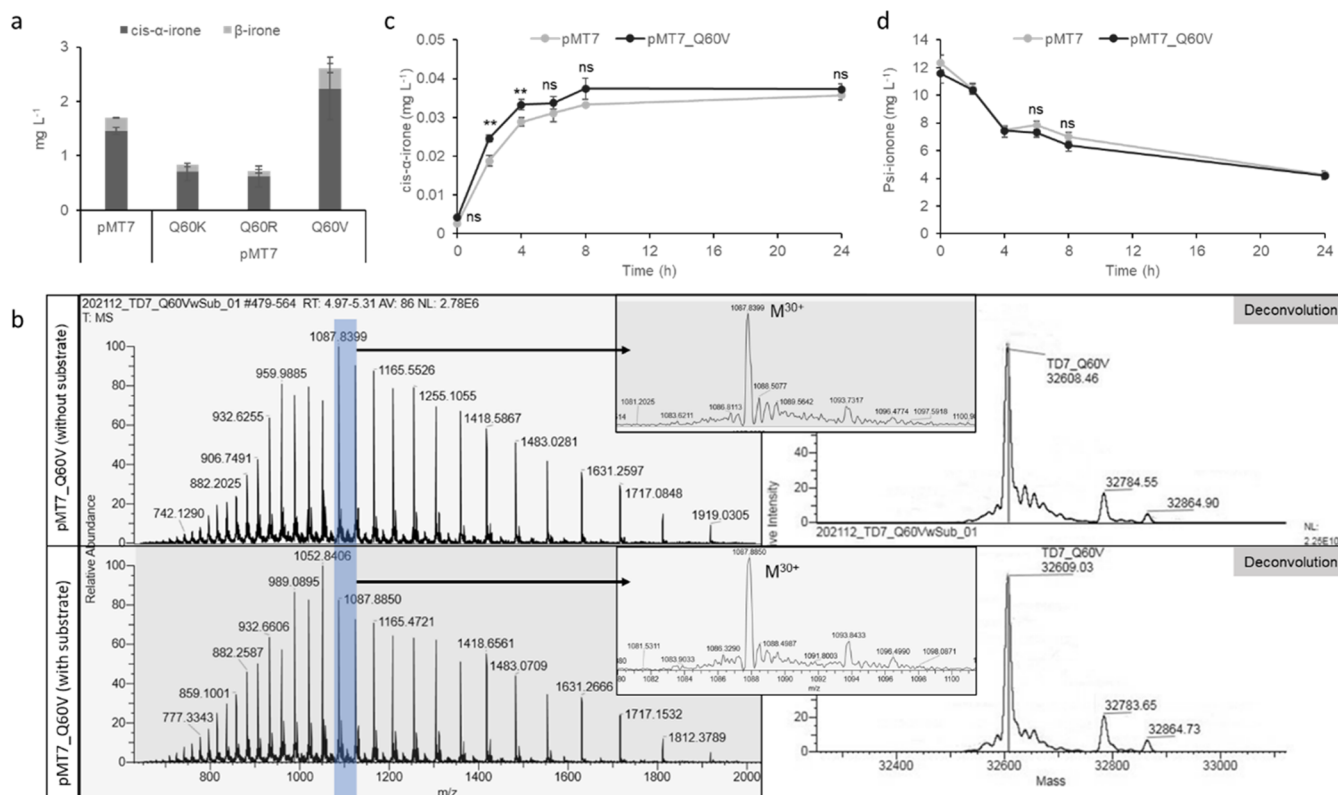


Figure 4. Mutagenesis of Q60 improved enzymatic activity and abolished the strong interaction between ψ -ionone and pMT7. (a) *cis*- α -Irene and β -irone production by each mutant enzyme in cell lysate was quantified by GCMS. The average and the standard deviation (s.d.) of two biologically independent experiments are shown. (b) Mass spectrum and deconvoluted mass of purified pMT7_Q60V showed the same proteoform profile in both samples with or without the substrate. Time course of purified pMT7 and pMT7_Q60V reactions for (c) *cis*- α -irone production and (d) ψ -ionone consumption. The average and the standard deviation (s.d.) of three biologically independent experiments are shown. Significance (*p*-value) was evaluated by two-sided student's *t*-test: ns, *p* > 0.05; **p* < 0.05; ***p* < 0.01; ****p* < 0.001; *****p* < 0.0001.

Table 1. Kinetics Parameters of pMT Mutant Enzymes

	substrate	K_m (μ M)	k_{cat} ($\times 10^3$ h ⁻¹)	k_{cat}/K_m (M ⁻¹ s ⁻¹)	ref
pMT7	ψ -ionone	24.9 \pm 3.7	2.2 \pm 0.11	0.024	3
	SAM	53.6 \pm 1.8	2.6 \pm 0.025	0.013	
pMT7_Q60V	ψ -ionone	56.9 \pm 1.9	5.1 \pm 0.05	0.025	this study
	SAM	37.3 \pm 1.1	5.3 \pm 0.05	0.039	
pMT10	ψ -ionone	18.1 \pm 0.03	19.9 \pm 0.1	0.30	3
	SAM	31.4 \pm 2.4	25.8 \pm 0.47	0.23	
pMT12	ψ -ionone	119.5 \pm 4.8	96.3 \pm 2.0	0.22	this study
	SAM	43.1 \pm 1.7	43.3 \pm 1.1	0.28	
pMT12_Q60V	ψ -ionone	104.1 \pm 0.7	83.8 \pm 0.7	0.22	this study
	SAM	80.7 \pm 1.0	55.7 \pm 0.9	0.19	

is abolished in the presence of Q60V mutation. This was surprising given the Q60 residue is far away from the active site.

To understand the effect of Q60V mutation, molecular dynamics simulations were performed with both pMT7 and pMT7_Q60V, and root mean square fluctuations (RMSF) were computed for all of the amino acid residues. Our simulations indicate that overall, RMSF values are higher for pMT7 than those for pMT7_Q60V (Supporting Figure S2a). In particular, the dimer interchain loop (residues 41-52: WFPPDAPVPQDM) showed lower RMSF values for pMT7_Q60V, suggesting a stabilization of the dimer interface. The root mean square deviation (RMSD) computed along the MD simulations also revealed a global stabilization of the enzyme dimer by nearly 1 Å upon introduction of Q60V

mutation (Supporting Figure S2b). Detailed inspection along the simulation of the interactions involving Q60 or V60, Q62, and surrounding residues, notably from the interchain loop W41-M52, revealed the loss of interaction between Q60 and the neighboring R64 and the formation of strong ionic interactions between R64 with D45 from both chains when Q60 was mutated to valine (Figure 3b). On the other hand, V60 is stabilized by additional van der Waals interactions with hydrophobic side chains of residues F42, A46, P47, and P49 from the interchain loop W41-M52. Interestingly, the loop W41-M52 was also found to be stabilized by two hydrogen bonding interactions between the N231 side chain from the other chain (chain B) and the backbone amide from W41 and F42 residues. The dynamics of loop W41-M52 at the interface between the two chains of the dimer appears to play an

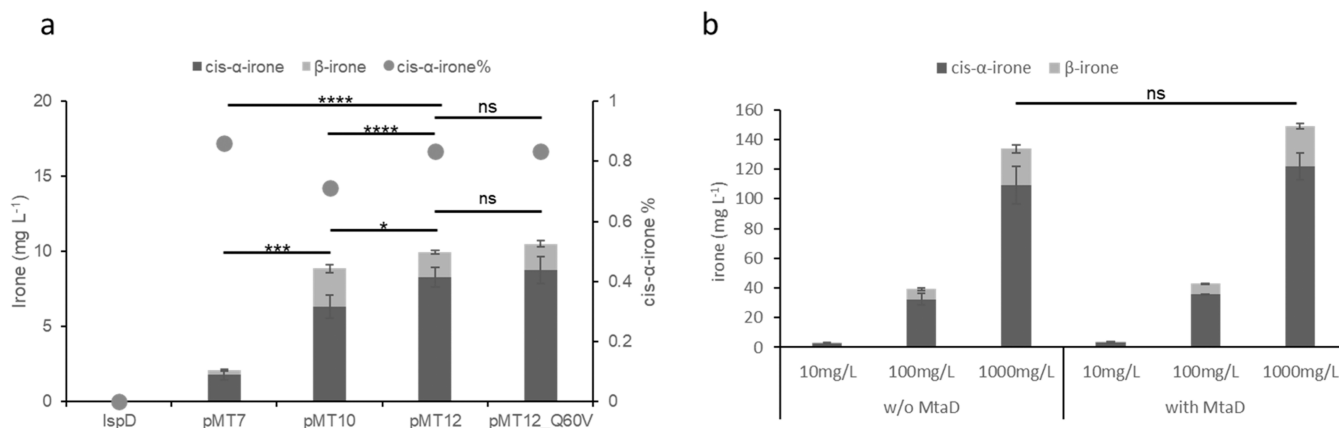


Figure 5. In vitro biotransformation of psi-ionone to *cis*- α -irone. (a) *cis*- α -irone and β -irone production by each mutant enzyme in cell lysate was quantified by GCMS. 40 mg L⁻¹ psi-ionone and 0.2 mM SAM were added at the start of the reaction. The percentage of *cis*- α -irone was calculated by dividing *cis*- α -irone concentration by the total irone concentration. (b) Production of irone by the pMT12 enzyme in cell lysate when different starting amounts of psi-ionone were used. For both (a) and (b), the average and the standard deviation (s.d.) of three biologically independent experiments are shown. Significance (*p*-value) was evaluated by two-sided student's *t*-test: ns, *p* > 0.05; **p* < 0.05; ***p* < 0.01; ****p* < 0.001; *****p* < 0.0001.

important role in stabilizing the enzyme. The improved activity of pMT7_Q60V compared to pMT7 (Figure 4a) might be attributed to the stabilization of pMT7_Q60V observed by molecular modeling.

Next, we tested if Q60V mutation could prolong the enzymatic activity and achieve higher irone production before reaching a plateau. The time course of reactions performed using purified pMT7 and pMT7_Q60V is shown in Figure 4c. The rate of irone production was found to be faster with the pMT7_Q60V mutant, but similar amounts of irone were produced at the end of 24 h incubation by both enzymes (Figure 4c). Moreover, both reactions reached a plateau after 8 h, before significant conversion was achieved. The estimated amount of SAH produced is $\sim 0.2 \mu\text{M}$, which is not yet at the inhibitory concentration. Also, the Native PAGE gel showed that the enzyme remained as a hexamer after the reaction, suggesting that the mutation did not alter the oligomeric state of the methyltransferase and the enzyme is stable under the reaction conditions (Supporting Figure S3). It is also observed that during protein fractionation, approximately 10% of the protein was modified, suggesting that the strong interaction between psi-ionone and pMT7 might attribute to a small percentage of the total activity loss. Therefore, other inactivation mechanisms remain to be explored. We have also quantified the consumption of psi-ionone, which also showed a higher rate of decrease with the pMT7_Q60V mutant at 4–6 h (Figure 4d). It is interesting to note that the decrease of psi-ionone concentration ($\sim 3\text{--}6 \mu\text{M h}^{-1}$) is much faster than the production of irone ($\sim 0.035\text{--}0.06 \mu\text{M h}^{-1}$), suggesting that psi-ionone might be degraded in the solution.

Mutagenesis of Dimer Interchain Residues Improved Enzyme Specificity. As the introduction of Q60V mutation stabilizes the enzyme by likely perturbing the interaction network between residue 60 and the loop W41-M52 at the dimer interface, we hypothesized that mutating N231, which forms two hydrogen bonds with the loop, might alter the enzymatic property (Figure 3b). Site saturation mutagenesis was then performed at position N231 using pMT7 as a template. Unfortunately, none of the mutations were found to be beneficial to improve the enzymatic activity, although we noticed that N231D and N231Q altered the enzyme specificity

by increasing the percentage of *cis*- α -irone in the product mixture (Supporting Figure S4). Moreover, N231D mutation only resulted in a slight reduction in activity compared to pMT7. Therefore, we considered this mutation to be promising to further enhance the specificity of pMT10, which is more active but less specific than pMT7. Indeed, combining N231D mutation into pMT10 led to an increase of the percentage of *cis*- α -irone from ~ 70 to $\sim 83\%$, even though the total amount of irone produced remained similar (Figure 5a and Supporting Figure S5).

While we were investigating the dimer interface residues, we also attempted to increase the specificity of the pMT10 mutant. pMT10 has two additional mutations based on pMT7: C156A and T91P. Site saturation mutagenesis of the T91 residue based on pMT10 did not yield any improved mutants. Site saturation mutagenesis of C156 has been performed based on the pMT6 mutant in our previous study,³ so only selected mutations (C156D and C156G) were tested based on pMT10. Mutating C156 to aspartate instead of alanine in pMT10 shifted the product distribution toward *cis*- α -irone without changing the total irone production (Supporting Figure S5). Subsequently, we introduced both N231D and C156D mutations in pMT10 and generated the pMT12 mutant that increased the total *cis*- α -irone production by ~ 4.7 - and ~ 1.3 -fold compared to pMT7 and pMT10, respectively (Figure 5). The k_{cat} of pMT12 was $\sim 16\text{--}44$ fold higher than that of pMT7 and $\sim 1.6\text{--}4.8$ -fold higher than that of pMT10, suggesting a synergistic effect of both mutations (Table 1). Moreover, the *cis*- α -irone percentage has increased to $\sim 83\%$ by pMT12, which is higher than pMT10 but lower than pMT7. Therefore, mutations that alter the enzyme specificity can be further explored. In addition to pMT12, we also introduced Q60V mutation (pMT12_Q60V) to test if the enzymatic activity can be further increased. However, the *cis*- α -irone concentration increase was marginal at the end of 72 h incubation (Figure 5a). Based on kinetic characterization, we observed similar catalytic efficiency, namely, k_{cat}/K_m , for psi-ionone between pMT12 and pMT12_Q60V, whereas that of SAM for pMT12_Q60V decreased slightly compared to pMT12 (Table 1). Structurally, both pMT12 and pMT12_Q60V remained as hexamers after the reaction based on the native

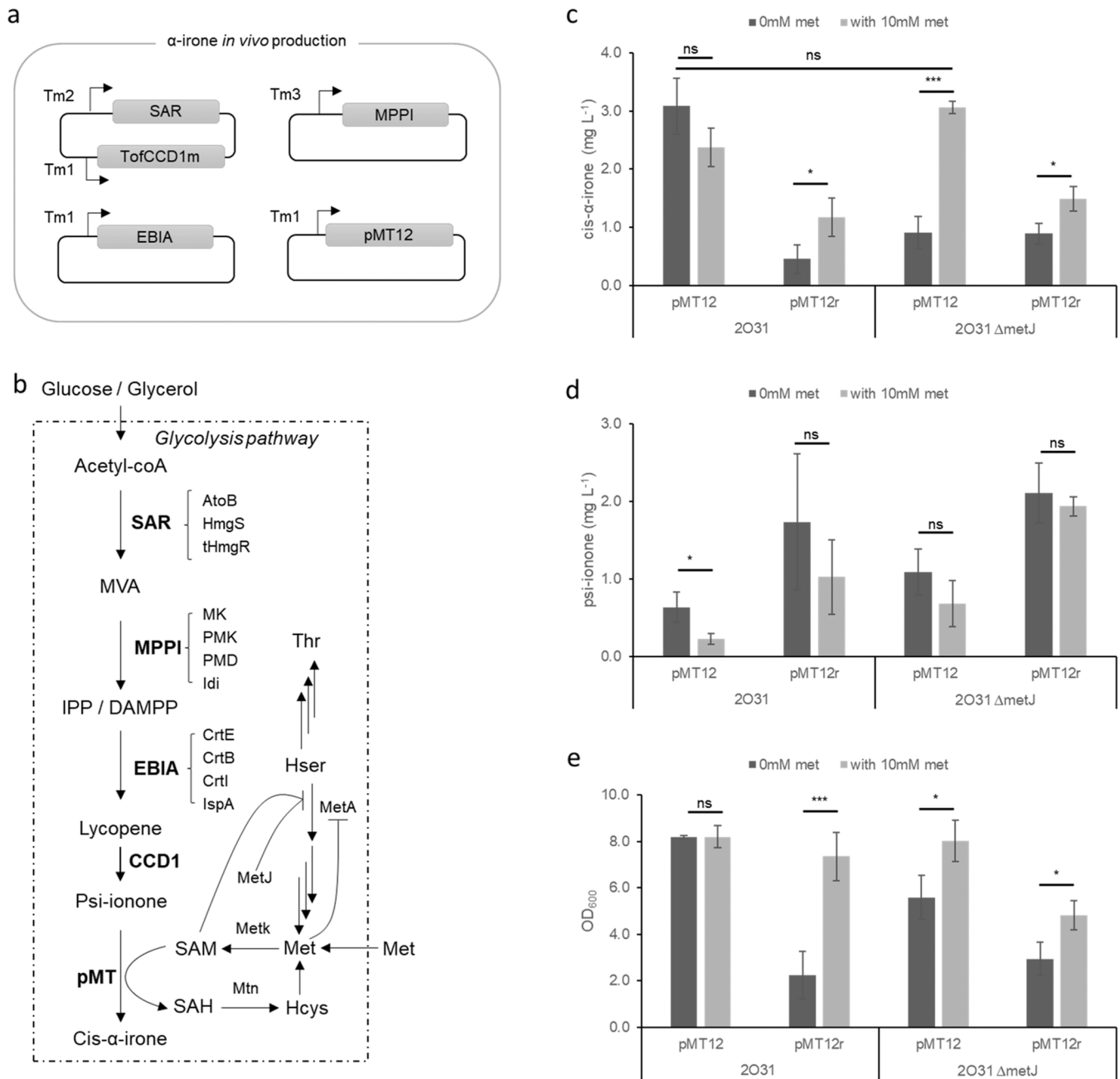


Figure 6. *In vivo* production of *cis-α*-irone from a simple carbon source. (a) Schematic representation of the plasmids used to produce *cis-α*-irone (Supporting Table S1). Tm1, Tm2, and Tm3 are the mutated T7 promoters with different strengths (Tm1 > Tm2 > Tm3)²⁵ (b) Schematic representation of the pathway to convert the simple carbon source to *cis-α*-irone. The proposed pathway involved in methionine biosynthesis and regulation is also illustrated. The cell membrane is represented by the dotted line. Refer to the Abbreviation section for the full gene names and metabolites in the pathway. The bar charts represent the average amount of *cis-α*-irone produced in (c); the average amount of leftover psi-ionone in (d); and the average final biomass in (e) when genetic and abiotic optimization was carried out. The average and the s.d. of three biologically independent experiments are shown. Significance (*p*-value) was evaluated by two-sided student's *t*-test: ns, *p* > 0.05; **p* < 0.05; ***p* < 0.01; ****p* < 0.001; *****p* < 0.0001. pMT12 refers to the overexpression of pMT12 only in the 2O31 strain. pMT12r refers to the overexpression of pMT12, MetK, and Mtn in the 2O31 strain. Refer to Supporting Table S1 for the full strain description.

PAGE gel analysis, suggesting that the additional mutations did not alter the oligomeric state of the methyltransferase (Supporting Figure S3). To understand the effect of mutations, molecular dynamics simulations were again performed on pMT12 and pMT12_Q60V. As introduction of N231D mutations still allowed formation of hydrogen bonding interactions with the backbone amide of W41 and F42 from the dimer interchain loop, we did not observe considerable differences in the RMSF of loop W41-M52 in both pMT12

and pMT12_Q60V compared to pMT7_Q60V (Supporting Figure S2a). Comparing between pMT12 and pMT12_Q60V mutants, the Q60V mutation seemed to have little effect on the global protein stability based on RMSD analysis, even though there is a similar but marginal stabilizing effect observed for the dimer interchain loop W41-M52 based on RMSF analysis (Supporting Figure S2).

Since pMT12 has a higher catalytic efficiency for SAM than pMT12_Q60V, pMT12 was used for further *in vitro*

production of *cis*- α -irone from *psi*-ionone. To challenge the mutant enzyme, we supplemented 10 mg L⁻¹ (0.05 mM), 100 mg L⁻¹ (0.5 mM), or 1000 mg L⁻¹ (5 mM) *psi*-ionone into the cell lysates containing overexpressed pMT12 and ~2.8 mg L⁻¹ (~0.014 mM), 32.5 mg L⁻¹ (~0.16 mM), and 109.3 mg L⁻¹ (~0.53 mM) *cis*- α -irone were produced, respectively, after incubating the reaction mixture at 28 °C for 3 days³ (Figure 5b). At the same time, ~0.55, ~6.6, and ~24.4 mg L⁻¹ β -irone was also produced, respectively. In our previous study, we supplemented *S*-adenosylhomocysteine deaminase (MtaD), which converted SAH to *S*-inosyl-homocysteine and ammonia, into the pMT10 reaction to alleviate the SAH inhibition to pMT10 and observed that SAH could be effectively removed by the endogenous *S*-adenosylhomocysteine nucleosidase (Mtn) present in the cell lysate.³ Mtn is a part of the methionine cycle enzymes that converts SAH to *S*-ribosyl-homocysteine and adenine. Similarly, we introduced the MtaD enzyme in the pMT12 reaction. Here, we observed a slight increase in *cis*- α -irone production to ~121.8 mg L⁻¹ and in β -irone production to ~27.3 mg L⁻¹ when MtaD was supplemented in the reaction with 1000 mg L⁻¹ *psi*-ionone, suggesting that the presence of the endogenous Mtn enzyme in cell lysate might become limiting.

In Vivo Biotransformation. To economically regenerate the SAM cofactor, the optimized pMT enzyme was incorporated into the 2O31 strain to produce irone directly from simple carbon sources (Figure 6a,b). After three-day incubation, both pMT12 and pMT12_Q60V produced ~3 mg L⁻¹ *cis*- α -irone, which was ~74% higher than the product concentration of the pMT10-containing strain (Supporting Figure S6). The unreacted *psi*-ionone amount was also reduced by pMT12 and pMT12_Q60V. Since pMT12 produced a slightly higher amount of *cis*- α -irone and *psi*-ionone, we used pMT12 to further optimize in vivo production of *cis*- α -irone. Both genetic modification and abiotic condition optimization were carried out by (1) overexpressing the methionine cycle enzymes, MetK and Mtn, (2) deleting the transcriptional regulator *metJ*, and (3) supplementing 10 mM methionine in growth media. However, none of the strategies enabled to improve *cis*- α -irone production (Figure 6c). Similar to our previous study,³ when methionine cycle enzymes were overexpressed (pMT12r, Supporting Table S1), the *cis*- α -irone production decreased significantly with concomitant accumulation of *psi*-ionone (Figure 6c,d). For *metJ* deletion, the leftover *psi*-ionone was generally higher in the 2O31 Δ *metJ* strain than the 2O31 strain (Figure 6d), but the highest amount of *cis*- α -irone produced in the 2O31 Δ *metJ* strain did not increase beyond ~3 mg L⁻¹ (Figure 6c). With 10 mM methionine supplementation, *cis*- α -irone production was generally improved for all of the strains except the 2O31 strain without overexpressing the methionine cycle enzymes (pMT12, Figure 6c and Supporting Table S1). It is interesting to note that when the methionine cycle enzymes were overexpressed, the biomass decreased significantly and was only restored with the addition of methionine (Figure 6e). This might be because methionine was rapidly converted to SAM with the MetK enzyme, and the methyltransferase enzymes were not fast enough to convert SAM to SAH, which is further converted back to methionine through the action of the Mtn enzyme (Figure 6b). The accumulation of SAM would inhibit the MetA enzyme, which was the first step in methionine biosynthesis,²⁴ further affecting the methionine biosynthesis (Figure 6b). Deleting *metJ* affected the growth of

the cell, too, which was restored with methionine addition (Figure 6e). Without *metJ*, MetA activity was shown to increase ~420-fold.²⁴ This might lead to uncontrolled flux from homoserine to methionine, rendering the cells unable to make sufficient threonine. When methionine was added, MetA activity was inhibited, allowing the flux to be redistributed between methionine and threonine biosynthesis (Figure 6b). When MetK and Mtn were overexpressed in 2O31 Δ *metJ* cells, an additive effect on biomass was observed as 10 mM methionine was insufficient to restore the cell growth (Figure 6e). A metabolomics study would be interesting to investigate the above hypotheses.

Taken together, our study employed mass spectrometry to examine the inactivation mechanism of the pMT7 reaction and identified a residue, Q60, at the dimer interface and away from the active site that was involved in forming a strong interaction with the substrate *psi*-ionone. Mutating Q60 to valine abolished the interaction and improved the k_{cat} by >2-fold compared to pMT7. The structural analysis further led us to identify another residue N231, which after mutating to aspartate increased the *cis*- α -irone percentage in the final product from ~70 to ~83%. The best mutant, pMT12, produced ~121.8 mg L⁻¹ *cis*- α -irone and 27.3 mg L⁻¹ β -irone from *psi*-ionone, which is a step closer to producing this premium fragrance molecule via biotransformation. Our results demonstrated that mutating residues involved in interactions at the dimer interface could lead to the improvement of both enzymatic activity and specificity. Additional mutations that stabilize the dimer interchain loop may lead to further activity enhancement. Our study offers a new strategy to engineer enzymes beyond the active site residues.

■ ASSOCIATED CONTENT

Supporting Information

The Supporting Information is available free of charge at <https://pubs.acs.org/doi/10.1021/acs.jafc.3c01272>.

Site saturation mutagenesis of Q60 and enabling identification of the amino acid residue involved in the strong interaction between *psi*-ionone and pMT7 (Figure S1); analysis of MD simulations of pMT enzymes and mutants (Figure S2); oligomeric state of pMT enzymes analyzed by native gel (Figure S3); site saturation mutagenesis of N231 based on pMT7 (Figure S4); mutations that improve the specificity of pMT10 (Figure S5); comparing in vivo production of *cis*- α -irone by pMT10, pMT12, and pMT12_Q60V (Figure S6); and strains and plasmids used in the study (Table S1) (PDF)

■ AUTHOR INFORMATION

Corresponding Author

Xixian Chen – Singapore Institute of Food and Biotechnology Innovation (SIFBI), Agency for Science, Technology and Research (A*STAR), Singapore 138669; orcid.org/0000-0002-0335-2058; Email: Xixian_chen@sifbi.a-star.edu.sg

Authors

Rehka T. – Singapore Institute of Food and Biotechnology Innovation (SIFBI), Agency for Science, Technology and Research (A*STAR), Singapore 138669

Xin Li – Protein and Proteomics Centre (PPC), Singapore's National Laboratory for Mass Spectrometry (SingMass), S2,

Level 2, Department of Biological Sciences, National University of Singapore, Singapore 117543

Jing Sen Ong – Singapore Institute of Food and Biotechnology Innovation (SIFBI), Agency for Science, Technology and Research (A*STAR), Singapore 138669

Jérémy Esque – Toulouse Biotechnology Institute, TBI, Université de Toulouse, CNRS, INRAE, INSA, F-31077 Toulouse, France

Congqiang Zhang – Singapore Institute of Food and Biotechnology Innovation (SIFBI), Agency for Science, Technology and Research (A*STAR), Singapore 138669; orcid.org/0000-0003-1070-8806

Qingsong Lin – Protein and Proteomics Centre (PPC), Singapore's National Laboratory for Mass Spectrometry (SingMass), S2, Level 2, Department of Biological Sciences, National University of Singapore, Singapore 117543; orcid.org/0000-0001-9117-8514

Isabelle André – Toulouse Biotechnology Institute, TBI, Université de Toulouse, CNRS, INRAE, INSA, F-31077 Toulouse, France; orcid.org/0000-0001-6280-4109

Complete contact information is available at: <https://pubs.acs.org/10.1021/acs.jafc.3c01272>

Notes

The authors declare the following competing financial interest(s): A PCT patent application (PCT/SG2022/050235) has been filed through the Agency for Science, Technology and Research.

ACKNOWLEDGMENTS

The authors would like to thank Dr. Ee Lui Ang, Dr. Nicholas David Lindley, and Dr. Hazel Khoo, the Singapore Institute of Food and Biotechnology Innovation for supporting this project. The authors acknowledge Singapore's National Laboratory for Mass Spectrometry (SingMass) for providing mass spectrometry and proteomic analysis. This work was granted access to High-Performance Computing (HPC) resources from the regional computing mesocenter CALMIP. This research is supported by the Agency for Science, Technology and Research (A*STAR) under Central Research Fund (Applied/Translational Research), AME Young Individual Research Grants: A1984c0040 (2018) and A2084c0064 (2019), and EcoCTs project supported by the National Research Foundation, Prime Minister's Office, Singapore under its Campus for Research Excellence and Technological Enterprise (CREATE) programme.

ABBREVIATIONS

pMT, promiscuous methyltransferase; HmgS, HMG-CoA synthase; AtoB, acetoacetyl-CoA thiolase; tHmgR, truncated HMG-CoA reductase; TofCCD1m, engineered OfCCD1 fused with thioredoxin; MK, mevalonate kinase; PMK, phosphomevalonate kinase; PMD, mevalonate pyrophosphate decarboxylase; Idi, isopentenyl pyrophosphate isomerase; CrtE, geranylgeranyl pyrophosphate synthase; CrtB, phytoene synthase; CrtI, phytoene desaturase; IspA, farnesyl pyrophosphate synthase; MetK, S-adenosylmethionine synthase; Mtn, S-adenosylhomocysteine nucleosidase; MetA, homoserine O-succinyltransferase; MtaD, S-adenosylhomocysteine deaminase; SAM, S-adenosylmethionine; SAH, S-adenosylhomocysteine; MVA, mevalonate; IPP, isopentenyl pyrophosphate; DMAPP, dimethylallyl pyrophosphate; Thr, threonine; Hser,

homoserine; Met, methionine; Hcys, homocysteine; Nuc, nucleophile; MD, molecular dynamics; RMSF, root mean square fluctuation; HS-SPME, headspace solid-phase microextraction; GCMS, gas chromatography–mass spectrometry

REFERENCES

- (1) Zhang, C.; Sultan, S. A.; T, R.; Chen, X. Biotechnological Applications of S-Adenosyl-Methionine-Dependent Methyltransferases for Natural Products Biosynthesis and Diversification. *Bioresour. Bioprocess.* **2021**, *8*, 72.
- (2) Ignea, C.; Raadam, M. H.; Koutsaviti, A.; Zhao, Y.; Duan, Y.-T.; Harizani, M.; Miettinen, K.; Georgantea, P.; Rosenfeldt, M.; Viejo-Ledesma, S. E.; Petersen, M. A.; Bredie, W. L. P.; Staerk, D.; Roussis, V.; Ioannou, E.; Kampranis, S. C. Expanding the Terpene Biosynthetic Code with Non-Canonical 16 Carbon Atom Building Blocks. *Nat. Commun.* **2022**, *13*, No. 5188.
- (3) Chen, X.; T, R.; Esque, J.; Zhang, C.; Shukal, S.; Lim, C. C.; Ong, L.; Smith, D.; André, I. Total Enzymatic Synthesis of Cis- α -Irone from a Simple Carbon Source. *Nat. Commun.* **2022**, *13*, No. 7421.
- (4) Chen, Z.; Shen, X.; Wang, J.; Wang, J.; Zhang, R.; Rey, J. F.; Yuan, Q.; Yan, Y. Establishing an Artificial Pathway for De Novo Biosynthesis of Vanillyl Alcohol in *Escherichia coli*. *ACS Synth. Biol.* **2017**, *6*, 1784–1792.
- (5) Yunus, I. S.; Palma, A.; Trudeau, D. L.; Tawfik, D. S.; Jones, P. R. Methanol-Free Biosynthesis of Fatty Acid Methyl Ester (FAME) in *Synechocystis* Sp. PCC 6803. *Metab. Eng.* **2020**, *57*, 217–227.
- (6) Ignea, C.; Pontini, M.; Motawia, M. S.; Maffei, M. E.; Makris, A. M.; Kampranis, S. C. Synthesis of 11-Carbon Terpenoids in Yeast Using Protein and Metabolic Engineering. *Nat. Chem. Biol.* **2018**, *14*, 1090.
- (7) Bennett, M. R.; Shepherd, S. A.; Cronin, V. A.; Micklefield, J. Recent Advances in Methyltransferase Biocatalysis. *Curr. Opin. Chem. Biol.* **2017**, *37*, 97–106.
- (8) Herbert, A. J.; Shepherd, S. A.; Cronin, V. A.; Bennett, M. R.; Sung, R.; Micklefield, J. Engineering Orthogonal Methyltransferases to Create Alternative Bioalkylation Pathways. *Angew. Chem., Int. Ed.* **2020**, *59*, 14950–14956.
- (9) Renata, H.; Lewis, R. D.; Sweredoski, M. J.; Moradian, A.; Hess, S.; Wang, Z. J.; Arnold, F. H. Identification of Mechanism-Based Inactivation in P450-Catalyzed Cyclopropanation Facilitates Engineering of Improved Enzymes. *J. Am. Chem. Soc.* **2016**, *138*, 12527–12533.
- (10) Warner, D. R.; Hoffman, J. L. Suicide Inactivation of Thioether S-Methyltransferase by Ethyl Vinyl Sulfide. *Biochemistry* **1996**, *35*, 4480–4484.
- (11) Lindahl, T.; Demple, B.; Robins, P. Suicide Inactivation of the *E. coli* O6-Methylguanine-DNA Methyltransferase. *EMBO J.* **1982**, *1*, 1359–1363.
- (12) Sen, S.; Mondal, S.; Zheng, L.; Salinger, A. J.; Fast, W.; Weerapana, E.; Thompson, P. R. Development of a Suicide Inhibition-Based Protein Labeling Strategy for Nicotinamide N-Methyltransferase. *ACS Chem. Biol.* **2019**, *14*, 613–618.
- (13) Shukal, S.; Lim, X. H.; Zhang, C.; Chen, X. Metabolic Engineering of *Escherichia coli* BL21 Strain Using Simplified CRISPR-Cas9 and Asymmetric Homology Arms Recombineering. *Microb. Cell Fact.* **2022**, *21*, 19.
- (14) Chen, X.; Shukal, S.; Zhang, C. Integrating Enzyme and Metabolic Engineering Tools for Enhanced α -Ionone Production. *J. Agric. Food Chem.* **2019**, *67*, 13451–13459.
- (15) Tang, L. W. T.; Verma, R. K.; Yong, R. P.; Li, X.; Wang, L.; Lin, Q.; Fan, H.; Chan, E. C. Y. Differential Reversible and Irreversible Interactions between Benzbromarone and Human Cytochrome P450s 3A4 and 3A5. *Mol. Pharmacol.* **2021**, *100*, 224–236.
- (16) Webb, B.; Sali, A. Comparative Protein Structure Modeling Using MODELLER. *Curr. Protoc. Bioinf.* **2016**, *54*, 5.6.1–5.6.37.
- (17) Maier, J. A.; Martinez, C.; Kasavajhala, K.; Wickstrom, L.; Hauser, K. E.; Simmerling, C. Ff145B: Improving the Accuracy of

Protein Side Chain and Backbone Parameters from Ff99SB. *J. Chem. Theory Comput.* **2015**, *11*, 3696–3713.

(18) Wang, J.; Wolf, R. M.; Caldwell, J. W.; Kollman, P. A.; Case, D. A. Development and Testing of a General Amber Force Field. *J. Comput. Chem.* **2004**, *25*, 1157–1174.

(19) Salomon-Ferrer, R.; Götz, A. W.; Poole, D.; Le Grand, S.; Walker, R. C. Routine Microsecond Molecular Dynamics Simulations with AMBER on GPUs. 2. Explicit Solvent Particle Mesh Ewald. *J. Chem. Theory Comput.* **2013**, *9*, 3878–3888.

(20) Jakalian, A.; Jack, D. B.; Bayly, C. I. Fast, efficient generation of high-quality atomic charges. AM1-BCC model: II. Parameterization and validation. *J. Comput. Chem.* **2002**, *23*, 1623–1641.

(21) Miller, B. R. I.; McGee, T. D., Jr.; Swails, J. M.; Homeyer, N.; Gohlke, H.; Roitberg, A. E. MMPBSA.py: An Efficient Program for End-State Free Energy Calculations. *J. Chem. Theory Comput.* **2012**, *8*, 3314–3321.

(22) Katoh, K.; Standley, D. M. MAFFT Multiple Sequence Alignment Software Version 7: Improvements in Performance and Usability. *Mol. Biol. Evol.* **2013**, *30*, 772–780.

(23) Crooks, G. E.; Hon, G.; Chandonia, J.-M.; Brenner, S. E. WebLogo: A Sequence Logo Generator. *Genome Res.* **2004**, *14*, 1188–1190.

(24) Usuda, Y.; Kurahashi, O. Effects of Dereglulation of Methionine Biosynthesis on Methionine Excretion in *Escherichia coli*. *Appl. Environ. Microbiol.* **2005**, *71*, 3228–3234.

(25) Zhang, C.; Seow, V. Y.; Chen, X.; Too, H.-P. Multidimensional Heuristic Process for High-Yield Production of Astaxanthin and Fragrance Molecules in *Escherichia coli*. *Nat. Commun.* **2018**, *9*, No. 1858.